Non-invasive Quantification of Whole-brain Cerebral Metabolic Rate of Oxygen by MRI

Feng Xu[1], **Yulin Ge**[2], and **Hanzhang Lu**[1,*]

[1] Advanced Imaging Research Center, University of Texas Southwestern Medical Center, Dallas, TX 75390

[2] Department of Radiology, New York University Medical Center, New York, NY 10016

Abstract

Cerebral metabolic rate of oxygen ($CMRO_2$) is an important marker for brain function and brain health. Existing techniques for quantification of $CMRO_2$ with Positron Emission Tomography (PET) or MRI involve special equipment and/or exogenous agent, and may not be suitable for routine clinical studies. In the present study, a non-invasive method is developed to estimate whole-brain $CMRO_2$ in humans. This method applies phase-contrast MRI for quantitative blood flow measurement and T2-Relaxation-Under-Spin-Tagging (TRUST) MRI for venous oxygenation estimation, and uses the Fick principle of arteriovenous difference for the calculation of $CMRO_2$. Whole-brain averaged $CMRO_2$ values in young, healthy subjects were 132.1±20.0 μmol/100g/min, in good agreement with literature reports using PET. Various acquisition strategies for phase-contrast and TRUST MRI were compared, and it was found that non-gated phase-contrast and sagittal sinus TRUST MRI were able to provide the most efficient and accurate estimation of $CMRO_2$. In addition, blood flow and venous oxygenation were found to be positively correlated across subjects. Owing to the non-invasive nature of this method, it may be a convenient and useful approach for assessment of brain metabolism in brain disorders as well as under various physiologic conditions.

Keywords

cerebral metabolic rate of oxygen; cerebral blood flow; venous oxygenation; TRUST MRI; internal jugular vein; sagittal sinus; phase contrast MRI

Introduction

The brain represents about 2% of the total body weight, but consumes about 20% of the total energy (1,2). The energy demand of the brain is met primarily by aerobic metabolism (3). Therefore, cerebral metabolic rate of oxygen ($CMRO_2$) is an important index of tissue viability and brain function. Many conditions are related to alterations in oxygen metabolism, such as Huntington's disease (4), Alzheimer's Disease (5) and normal aging (6). In addition, quantitative measurement of $CMRO_2$ is useful in understanding normal cerebral physiology during resting state, sleep, brain activation and physiologic challenges.

The measurement of $CMRO_2$ is not yet a routine procedure. Currently available techniques for $CMRO_2$ measurement require the infusion/injection/inhalation of exogenous agent. Positron Emission Tomography (PET) is a widely used technique using radioactively

[*]Corresponding Author: Hanzhang Lu, Ph.D. Advanced Imaging Research Center, UT Southwestern Medical Center, 5323 Harry Hines Blvd. Dallas, TX 75390, E-mail: hanzhang.lu@utsouthwestern.edu, Tel: 214-645-2761, Fax: 214-645-2744.

labeled ^{15}O (7). NMR methods use either ^{13}C-glucose (8,9) or ^{17}O-oxygen to estimate CMRO$_2$ (10,11), and are most often used in animal studies. Several reasons may have contributed to the difficulties in applying these techniques in routine clinical studies: 1) the procedure is quite invasive due to the use of exogenous agent with potential exposure to radiation (in PET) and the need of arterial/venous lines; 2) the relative long duration of the procedure that includes preparation, multiple injections, agent clearance, etc.; 3) the relatively high cost due to the need for special equipment (e.g. cyclotron) or special agent (e.g. ^{17}O). For studies of brain activation, an approach to estimate relative changes in CMRO$_2$, termed calibrated fMRI, has been developed (12–18), which measures neural activity induced BOLD and CBF changes and compares them to those induced by physiologic challenges such as hypercapnia (13–16) or hyperoxia (17). However, this approach only gives percentage changes in CMRO$_2$ associated with activation, but not absolute values in physiologic units. Therefore, like BOLD, the application of this method requires a "task". The baseline measurement alone has no clear physiologic correspondence. An additional confounding factor is that the method is based on the assumption of un-altered CMRO$_2$ during physiologic challenges, which is still under some controversy (19).

In this study, we utilized the Fick principle of arteriovenous oxygen difference, a principle used by Kety and Schmidt in their original CMRO$_2$ measurement (20) to quantify absolute CMRO$_2$ (in units of μmol/100g/min) in the whole brain non-invasively. Various parameters in the Fick equation were measured with MR techniques. Specifically, the venous blood oxygenation was estimated with a recently developed T2-Relaxation-Under-Spin-Tagging (TRUST) technique (21). Quantitative blood flow was estimated by phase-contrast MRI in the feeding arteries (22). Choices of optimal imaging strategies with considerations of accuracy and scan duration were investigated. The estimated CMRO$_2$ values were compared to literature results. While the proposed method only provides a global estimation of CMRO$_2$ but not regional distributions, it can offer quantitative and non-invasive measurements with duration of 5–10 minutes, and may find applications in conditions with whole brain alterations such as aging, sleep, sedation, hypercapnia, hyperoxia as well as in understanding resting state brain activities.

Materials and Methods

Theory for CMRO$_2$ estimation

Based on the Fick principle of arteriovenous difference in oxygen content, CMRO$_2$ can be written as (20):

$$CMRO_2 = CBF(Y_a - Y_v) \cdot C_a \tag{1}$$

where CBF is the amount of blood passing through the brain tissue in ml/100g/min, Y_a and Y_v are arterial and venous oxygenations (in %), respectively, C_a is a constant representing the amount of oxygen molecules that a unit volume of blood can carry. The value of C_a is reasonably well established in hematology and pulmonary physiology literature (23). Considering that each gram of hemoglobin can carry 55.6 μmol of oxygen (23) and there are 15 grams of hemoglobin in 100ml blood (at a typical hematocrit of 0.44) (23), the value of C_a is 833.7 μmol O$_2$/100ml blood. Under normal conditions, arterial blood is close to fully oxygenated, thus Y_a can be considered 100%. For studies of pathologic or special conditions (e.g. hypoxia), the arterial oxygenation can be easily measured with Pulse Oximeter.

Y_v and CBF in Eq. 1 will be estimated using MRI measurements. Recently, we have developed an approach to assess Y_v in venous vessels by TRUST MRI (21). Briefly, TRUST MRI utilizes the spin tagging principle to separate out the pure (venous) blood

signal by performing a pair of tag and control scans. The subtraction of the tag and control images then yields blood signal only. The tag and control scans are performed with various numbers of flow-insensitive T2-preparation pulses to modulate the signal with different T2-weightings. The monoexponential fitting of the blood signal to T2-preparation duration (termed effective TE, or eTE) then gives the T2 value of the venous blood, which is converted to Y_v using an in vitro calibration plot (24). CBF can be estimated by phase-contrast MRI or arterial-spin-labeling (ASL) MRI. In this study, we chose to use phase-contrast MRI for CBF quantification for two reasons: 1. Phase-contrast MRI in the feeding arteries can provide an estimation of the whole brain blood flow, which is in line with the whole brain Y_v estimation using TRUST MRI in large draining veins (e.g. sagittal sinus, internal jugular veins). 2. While ASL MRI can assess spatial distributions of blood flow to the brain, the quantification of CBF from ASL signal is less straightforward and is often dependent on transit time, labeling efficiency and trailing time (25–28). Phase-contrast MRI utilizes the phase of an image to encode the velocity of moving spins and has been widely used for angiogram and quantitative flow measurements (22).

MRI experiments

MR experiments were performed on a 3 Tesla MRI systems (Philips Medical Systems, Best, the Netherlands). The protocol was approved by Institutional Review Board of our University and informed written consent was obtained for each participant. A total of 36 healthy subjects (16 female, 20 male, age 42±20 years) participated in this study. Five subjects were used in the comparison of gated and non-gated phase-contrast MRI. In seventeen subjects, $CMRO_2$ was estimated using both sagittal sinus and internal jugular vein TRUST MRI. In the remaining fourteen subjects, only sagittal sinus TRUST MRI was used in $CMRO_2$ estimation. The body coil was used for RF transmission and an 8-channel SENSE head coil was used for receiving. Foam padding was used to stabilize the head to minimize motion. The subjects were instructed not to fall asleep during the experiments, and this was verified after each block of scans, because CBF and venous oxygenation may change during sleep (29).

Venous oxygenation levels of two major draining veins, sagittal sinus (SS) and internal jugular vein (IJV), were studied. The Y_v values and the estimation accuracy between these two venous locations were compared to determine the optimal location with most accurate estimation and minimum scan time. TRUST MRI on SS was performed with the following parameters: single-shot EPI, axial plane, voxel size = $3.44×3.44×5mm^3$, field of view (FOV) = $220×220×5mm^3$, repetition time (TR) = 8000ms, echo time (TE) = 19ms, inversion time (TI) = 1200ms, tagging slab thickness = 80mm, gap between imaging slab and tagging slab = 20mm,, four different T2-weightings with eTE of 0ms, 40ms, 80ms and 160ms, corresponding to 0, 4, 8 and 16 refocusing pulses in the T2-preparation (τ_{CPMG} =10 ms). For each eTE, four pairs of tag and control images were acquired to improve signal-to-noise ratio (SNR). The total scan time of SS TRUST MRI is 4 minutes and 16 seconds. TRUST MRI on IJV used similar parameters except for the following: two-shot EPI, voxel size = $2×2×10mm^3$, FOV = $160×160mm^2$, tagging thickness = 170mm, gap = 10mm, three different T2-weightings with eTE of 0ms, 40ms and 80ms. Compared to the SS TRUST MRI, the spatial resolution was slightly increased to allow the separation of IJV from several other vessels in the neck regions (e.g external jugular veins, venous plexuses, internal and external carotid arteries). To reduce EPI-related image distortions under high resolution, two-shot EPI was used. Consequently, the scan duration of IJV TRUST MRI was increased to 6 minutes and 24 seconds despite the reduction of eTE number from 4 to 3.

TRUST MRI planning for SS was based on middle sagittal survey image (Fig. 1a). It is relatively straightforward to identify the SS along the posterior boundary of occipital lobe located between brain and skull. The SS TRUST imaging slice is oriented axially

intersecting the SS at about 1 cm above the sinus congruence where the SS, straight sinus and transverse sinus join. The tagging slab is chosen to tag all the venous blood upstream of the imaging location. For scan planning of IJV, a time-of-flight (TOF) venogram was found necessary in order to reproducibly position the slices. The TOF venogram covered the sigmoid sinus as well as the upper part of the IJV with the following parameters: TR/TE/flip angle=23ms/3.45ms/18°, FOV=$160\times70\times160$mm^3, voxel size $1.0\times1.0\times1.5$mm^3, number of slices =47, one saturation slab of 60mm positioned below the imaging slab, duration 1 min 26 sec. Based on the sagittal and coronal views of maximum intensity projection (MIP) of the venogram (Fig. 1b), imaging slice of TRUST MRI was positioned to cover the IJV immediately below the jugular bulb, where the vein exits the cranial cavity.

For phase-contrast MRI, non-gated and cardiac-gated implementations were compared to determine the optimal sequence. Non-gated phase-contrast MRI is relatively short in scan duration but the image tends to have cardiac pulsation artifacts. The gated sequence can provide artifact-free velocity maps at different cardiac phases, but takes much longer time. For both gated and non-gated scans, the following parameters were used: single slice, voxel size = $0.45\times0.45\times5$ mm^3, FOV = $230\times230\times5$ mm^3, maximum velocity encoding = 80 cm/s. The non-gated scan results in one phase-contrast image with scan duration of 30 seconds. The gated scan results in 15 images at different cardiac phases with scan duration around 5 minutes and 30 seconds depending on subject's heart rate. The positioning of the phase-contrast scan was based on a TOF angiogram (acquired with similar parameters as the venogram described above except for opposite location of saturation slab) and the slice was oriented perpendicular to the internal carotid and vertebral arteries (Fig. 1c).

In addition, a T1-weighted MPRAGE image (voxel size $1\times1\times1$ mm^3) was acquired to provide an estimation of the intracranial volume, so that blood flow per unit mass of tissue can be calculated, which accounts for the variances in brain sizes across subjects.

Data analysis

Data were processed using in-house MATLAB (Mathworks, Natick, MA) scripts. The data processing procedures for TRUST MRI are based on an algorithm described previously (21). Briefly, after pair-wise subtraction between control and tag images, a preliminary ROI was manually drawn to include the target veins. This ROI tends to have about 30–50 voxels which include the veins as well as some surrounding tissue. To further define the venous voxels, the voxels with highest blood signals (according to the difference signals) in the ROI were chosen as the final mask for spatial averaging. For the purpose of standardizing protocol, we used 4 voxels for SS and 10 voxels for IJVs, although we have tested the effect of voxel number and found that the results are relatively insensitive to the number (21). The number of voxels used was greater in the IJV scan because the scan has smaller voxel size. This way the total area included is comparable to that in the SS scan. The venous blood signals were fitted to a mono-exponential function to obtain T2. The T2 was in turn converted to Y_v via a calibration plot (21) obtained by in vitro bovine blood experiments under controlled oxygenation, temperature and hematocrit conditions (24,30). In addition, the standard error (SE) of the estimated parameters was calculated based on a goodness-of-fit procedure (Matlab routine nlparci.m).

For phase-contrast MRI data, a preliminary ROI was drawn on each of the four arteries (left and right internal carotid arteries, left and right vertebral arteries) based on the magnitude image. A signal intensity threshold was then applied to the magnitude image to obtain the final vessel mask. For non-gated phase-contrast image, the threshold was set to be 5 times the background noise. For the gated scan, threshold was applied on each of the cardiac phases and the threshold value was reduced to 3.5 times the noise, in order to account for the lower SNR in the gated scan. This mask was applied to the phase image (velocity map) (Fig.

2) to yield the whole brain blood flow. The unit volume CBF (in ml/100g/min) was then obtained by normalizing the total CBF to the intracranial volume, which was estimated from the high resolution T1 weighted image using FSL (FMRIB Software Library, Oxford University) functions (BET,, FLIRT, BETSURF).

Results

Figures 2b and d show the velocity maps for non-gated and gated phase-contrast scan, respectively. Cardiac-pulsation-induced ghosting can be seen in the non-gated image (green arrows), whereas the gated image is free to these artifacts. There is a clear fluctuation of whole-brain CBF within the cardiac cycle (Fig. 2e). The averaged whole brain flow was 662 ± 118 ml/min (mean$\pm$SD, n=5), which is not significantly different from the values, 679 ± 73 ml/min, using the non-gated scan (paired t test, p=0.53). Therefore, given the considerable difference in scan duration (5.5 min and 0.5 min for gated and non-gated scan, respectively), the non-gated phase-contrast sequence was used in all other experiments.

Results of SS and IJV TRUST MRI are illustrated in Fig. 3. The control (Figs. 3a and d) and tag (Figs. 3b and e) images are almost identical and the locations of the veins are not obvious. Subtraction between these images highlighted the venous blood signal shown as bright voxels in the difference images (Figs. 3c and f), suggesting an effective tagging of the targeted vessels in both SS and IJV scans. The Y_v in SS and IJV were found to be $62.8\pm5.3\%$ (n=17) and $64.6\pm5.4\%$, respectively. Inter-subject variations in Y_v values are seen in both SS and IJV data, and furthermore the Y_v in SS and IJV shows a significant correlation (cc=0.71, p= 0.0015) (Fig. 3g). The standard errors of Y_v estimations were $1.6\pm0.9\%$ and $1.6\pm0.9\%$ for SS and IJV, respectively. These estimation errors show no significant difference between the two venous locations (p=0.95), suggesting that the estimation accuracy are comparable between the SS and IJV TRUST scans. No difference was observed between Y_v in SS and IJV (paired t-test, p=0.09). We considered that the IJV TRUST MRI requires a longer scan duration compared to SS TRUST and also needs a venogram as a localizer, all together taking approximately 9 minutes, which is twice the duration of the SS TRUST scan. Thus, SS TRUST MRI was used in all later experiments.

Combining the phase-contrast MRI and TRUST MRI measurements and utilizing Eq. 1, whole brain averaged $CMRO_2$ was estimated. Table 1 summarizes the $CMRO_2$ results. The estimated $CMRO_2$ values are in good agreement with previous PET studies (Table 2).

Given the different brain physiology that CBF, Y_v (i.e. OEF) and CMRO2 represent, it would be of interest to examine whether they have intrinsic correlations across subjects. Experiments were therefore performed in additional subjects and the scatter plot of these parameters were studied (Fig. 4). It can be seen that the blood flow and venous oxygenation are highly correlated (cc=0.65, p<0.0001, Fig. 4a) across subjects, and that subjects with higher blood flow tend to have higher Y_v. Similarly, CBF and CMRO2 also showed a trend of positive correlation (cc=0.41, p=0.0222, Fig. 4b), although the level of statistical significance is lower. No correlation was observed between Y_v and CMRO2.

Discussion

This study presents an MRI approach to quantify absolute cerebral metabolic rate of oxygen (in units of μmol O_2/100g brain/min) in humans. The main advantages of the proposed method are that it is completely non-invasive and can be performed with duration of 5–10 minutes on a standard clinical scanner. To our knowledge, this is the first approach to assess $CMRO_2$ without any exogenous agents (e.g. radioactive tracers in PET (7), ^{13}C (8), ^{17}O tracers (10) or Gd-DTPA contrast agent (31) in MRI). The whole-brain averaged $CMRO_2$

values were 132.1±20.0 μmol/100g/min, in good agreement with literature reports using PET. This measurement was achieved using a quantitative phase-contrast flow measurement in combination with a recently developed venous oxygenation technique (21).

Because the accuracy of the $CMRO_2$ estimation is critically dependent on the validity of the individual MRI measurements, each of the MR techniques was assessed in terms of optimal acquisition strategies. The gated and non-gated phase-contrast MRI were compared for the flow quantification, and it was found that the non-gated scan can provide an estimation of total blood flow similar to that using the gated scan. This result is consistent with the finding from a previous study, which showed a difference of 3% between the two techniques (32). Considering a >10 fold difference in scan duration (30s vs. 5.5 minutes), we recommend the non-gated phase-contrast scan for future studies. TRUST MRI in SS and IJV demonstrated that the blood oxygenation in SS and IJV are highly correlated across subjects. This is expected because the general venous flow trajectory is from venous sinuses to jugular veins (although some venous blood in sinuses leaves the intracranial space via venous plexuses and dural emissary veins (33). The estimation accuracy as assessed by standard errors is comparable for both methods. The estimation accuracy is also relatively insensitive to the spatial gap between imaging slice and labeling slab. We have compared Yv in SS TRUST using gaps of 10, 15, 20mm, and found virtually identical values. Since the IJV measurement takes about twice the time of the SS scan (see Methods and Results for details), we recommend the SS Y_v measurements for future studies. Therefore, our current protocol takes about 7 minutes for the whole-brain $CMRO_2$ measurement which includes the following MR sequences: TOF angiogram (2 minutes), SS TRUST MRI (4.5 minutes), non-gated phase-contrast MRI (0.5 minute).

Scan duration of seven minutes is still considered a relatively long time in a clinical study. In order to further reduce the time for the $CMRO_2$ measurement, several strategies can be used. First, the TOF angiogram is only used for localization of the feeding arteries and positioning of the phase-contrast MRI, but is not used in the actual calculation of $CMRO_2$. Thus, if one can use alternative anatomic landmarks such as vertebral bones or magnum foramen for the positioning of the phase-contrast scan, the angiogram can be omitted and the scan duration can be shortened by two minutes. However, this requires the MR operator to be quite familiar with the anatomic structures in the neck region. A second strategy to reduce the duration is to shorten the time for TRUST MRI. In the present protocol, TRUST MRI takes 4 minutes and 16 seconds which acquires four eTE weightings with each eTE having four repetitions. Therefore, one can reduce the number of eTEs and/or the number of repetitions. However, this is achieved at the cost of reducing estimation accuracy. We have performed analysis to investigate the dependence of estimation errors on repetition number and eTE number. We found that the reduction of repetition number and eTE number reduces the estimation accuracy in a similar manner. Thus, we have grouped them together and plotted the estimation error as a function of scan duration (TR × repetition number × eTE number × 2) (Fig. 5). It can be seen that the relationship between estimation error and the TRUST scan duration is not linear. The optimal protocol for each study should be based on how much scan time is available and what the acceptable estimation error is.

The present study utilized the effect of deoxyhemoglobin on blood T2 to estimate the venous oxygenation, a principle used be several previous studies (34–36). It should be noted that blood oxygenation can also be estimated based on the phase of blood magnetization, as demonstrated by Haacke et al. (37) and Fernandez-Seara et al. (38). In addition, based on theoretical framework developed by Yablonskiy and colleagues (39), An et al. (40) and He et al. (41,42) have shown that the effect of deoxyhemoglobin on extravascular tissue can be used for quantification of venous oxygenation. These approaches also have the potential to be used for quantitative estimation for CMRO2.

The proposed technique has a few limitations. First, the method only measures whole brain $CMRO_2$ but not a map of $CMRO_2$. Thus, it cannot provide regional $CMRO_2$ information. As a result, this technique will have limited utility in brain diseases with focal metabolic changes, such as acute stroke and brain tumor, unless the lesion regions cover the majority of the brain. To achieve spatially specific CMRO2 measurement, one would need mapping techniques for both CBF and Yv. CBF map can be obtained with arterial spin labeling MRI. For Yv, however, robust mapping measurement is still challenging. The TRUST method can be potentially applied to small veins or venules to estimate local Yv. However, one would need to develop a method to label the tissue and wait for the labeled spin to enter the venules, where its T2 is determined. In this regard, tissue-based techniques, such as the ones used by An et al. (40) and He et al. (41,42), may have an advantage if the biophysical model used can be shown to be applicable for all vessel sizes and orientations. Alternatively, 17O-based spectroscopy method may also prove to be valuable if the cost of 17O can be considerably reduced (10). Second, the effect of hematocrit (Hct) variations is not considered in this study. Hct will affect the estimation of Y_a-Y_v and C_a in Eq. 1. The calculation used in this study was based on Hct level of 0.44. If the actual Hct is higher than 0.44, Y_a-Y_v will be over-estimated, while C_a will be under-estimated (see Appendix for details). Numerical simulations were performed and it was found that, within the typical Hct range of 0.38 to 0.50, the bias in the estimated $CMRO_2$ was −5.6 to 7.1% of the true value (Fig. 6). To correct for this bias, one can measure the Hct of each individual by blood sampling. Finally, the proposed technique has not been validated with a gold standard method. While the estimated values are in good agreement with previous reports using radioactive tracers, each of the experimental measures in our MR method needs to be validated in order for this method to be routinely used in clinical settings. The flow measurement may be compared to perfusion-CT or Doppler techniques. The oxygenation measurement can be validated by blood sampling from the jugular vein. Alternatively, the entire method can be validated with respective PET techniques (e.g. 15O-labled H2O for flow, 15O-labeled O2 for oxygen extraction fraction). These studies shall be the subject of future investigations.

Conclusion

This work shows that whole brain $CMRO_2$ can be quantified with non-invasive MRI techniques within duration of 5–10 minutes. This method applies phase-contrast MRI for quantitative flow measurement and TRUST MRI for venous oxygenation estimation, and uses the Fick principle for the calculation of $CMRO_2$. The measured $CMRO_2$ in healthy subjects shows good agreement with literature values obtained by PET techniques. Owing to the non-invasive nature of our method, it may be a convenient and useful approach for assessment of brain metabolism in brain disorders as well as under various physiologic conditions such as sleep, sedation, hypercapnia, hypoxia and normal aging.

Acknowledgments

References

1. Elia, M. Organ and tissue contribution to metabolic rate. In: Kinney, JM.; Tucker, HN., editors. Energy Metabolism: Tissue Determinants and Cellular Corollaries. New York: Raven Press Ltd; 1992. p. 61-77.

2. Attwell D, Laughlin SB. An energy budget for signaling in the grey matter of the brain. J Cereb Blood Flow Metab. 2001; 21:1133–1145. [PubMed: 11598490]

3. Fox PT, Raichle ME. Focal physiological uncoupling of cerebral blood flow and oxidative metabolism during somatosensory stimulation in human subjects. Proc Natl Acad Sci U S A. 1986; 83:1140–1144. [PubMed: 3485282]

4. Leenders KL, Palmer AJ, Quinn N, Clark JC, Firnau G, Garnett ES, Nahmias C, Jones T, Marsden CD. Brain dopamine metabolism in patients with Parkinson's disease measured with positron emission tomography. J Neurol Neurosurg Psychiatry. 1986; 49:853–860. [PubMed: 3091770]

5. Buckner RL, Snyder AZ, Shannon BJ, LaRossa G, Sachs R, Fotenos AF, Sheline YI, Klunk WE, Mathis CA, Morris JC, Mintun MA. Molecular, structural, and functional characterization of Alzheimer's disease: evidence for a relationship between default activity, amyloid, and memory. J Neurosci. 2005; 25:7709–7717. [PubMed: 16120771]

6. D'Esposito M, Deouell LY, Gazzaley A. Alterations in the BOLD fMRI signal with ageing and disease: a challenge for neuroimaging. Nat Rev Neurosci. 2003; 4:863–872. [PubMed: 14595398]

7. Mintun MA, Raichle ME, Martin WR, Herscovitch P. Brain oxygen utilization measured with O-15 radiotracers and positron emission tomography. J Nucl Med. 1984; 25:177–187. [PubMed: 6610032]

8. Hyder F, Chase JR, Behar KL, Mason GF, Siddeek M, Rothman DL, Shulman RG. Increased tricarboxylic acid cycle flux in rat brain during forepaw stimulation detected with 1H[13C]NMR. Proc Natl Acad Sci U S A. 1996; 93:7612–7617. [PubMed: 8755523]

9. Gruetter R, Seaquist ER, Ugurbil K. A mathematical model of compartmentalized neurotransmitter metabolism in the human brain. Am J Physiol Endocrinol Metab. 2001; 281:E100–112. [PubMed: 11404227]

10. Zhu XH, Zhang Y, Tian RX, Lei H, Zhang N, Zhang X, Merkle H, Ugurbil K, Chen W. Development of (17)O NMR approach for fast imaging of cerebral metabolic rate of oxygen in rat brain at high field. Proc Natl Acad Sci U S A. 2002; 99:13194–13199. [PubMed: 12242341]

11. Pekar J, Ligeti L, Ruttner Z, Lyon RC, Sinnwell TM, van Gelderen P, Fiat D, Moonen CT, McLaughlin AC. In vivo measurement of cerebral oxygen consumption and blood flow using 17O magnetic resonance imaging. Magn Reson Med. 1991; 21:313–319. [PubMed: 1745131]

12. Kim SG, Ugurbil K. Comparison of blood oxygenation and cerebral blood flow effects in fMRI: estimation of relative oxygen consumption change. Magn Reson Med. 1997; 38:59–65. [PubMed: 9211380]

13. Davis TL, Kwong KK, Weisskoff RM, Rosen BR. Calibrated functional MRI: mapping the dynamics of oxidative metabolism. Proc Natl Acad Sci U S A. 1998; 95:1834–1839. [PubMed: 9465103]

14. Hoge RD, Atkinson J, Gill B, Crelier GR, Marrett S, Pike GB. Investigation of BOLD signal dependence on cerebral blood flow and oxygen consumption: the deoxyhemoglobin dilution model. Magn Reson Med. 1999; 42:849–863. [PubMed: 10542343]

15. Chiarelli PA, Bulte DP, Piechnik S, Jezzard P. Sources of systematic bias in hypercapnia-calibrated functional MRI estimation of oxygen metabolism. Neuroimage. 2007; 34:35–43. [PubMed: 17029987]

16. Leontiev O, Buxton RB. Reproducibility of BOLD, perfusion, and CMRO2 measurements with calibrated-BOLD fMRI. Neuroimage. 2007; 35:175–184. [PubMed: 17208013]

17. Chiarelli PA, Bulte DP, Wise R, Gallichan D, Jezzard P. A calibration method for quantitative BOLD fMRI based on hyperoxia. Neuroimage. 2007; 37:808–820. [PubMed: 17632016]

18. Pasley BN, Inglis BA, Freeman RD. Analysis of oxygen metabolism implies a neural origin for the negative BOLD response in human visual cortex. Neuroimage. 2007; 36:269–276. [PubMed: 17113313]

19. Zappe AC, Uludag K, Oeltermann A, Ugurbil K, Logothetis NK. The Influence of Moderate Hypercapnia on Neural Activity in the Anesthetized Nonhuman Primate. Cereb Cortex. 2008 [Epub ahead of print].

20. Kety SS, Schmidt CF. The Effects of Altered Arterial Tensions of Carbon Dioxide and Oxygen on Cerebral Blood Flow and Cerebral Oxygen Consumption of Normal Young Men. J Clin Invest. 1948; 27:484–492.

21. Lu H, Ge Y. Quantitative evaluation of oxygenation in venous vessels using T2-Relaxation-Under-Spin-Tagging MRI. Magn Reson Med. 2008; 60:357–363. [PubMed: 18666116]

22. Haacke, EM.; Brown, RW.; Thompson, MR.; Venkatesan, R. Magnetic Resonance Imaging: Physical Principles and Sequence Design. Wiley-Liss; 1999. MR Angiography and Flow Quantification.

23. Guyton, AC.; Hall, JE. Respiration. In: Guyton, AC.; Hall, JE., editors. Textbook of Medical Physiology. 11. Saunders: Elsevier; 2005.

24. Zhao JM, Clingman CS, Narvainen MJ, Kauppinen RA, van Zijl PC. Oxygenation and hematocrit dependence of transverse relaxation rates of blood at 3T. Magn Reson Med. 2007; 58:592–597. [PubMed: 17763354]

25. Yang Y, Engelien W, Xu S, Gu H, Silbersweig DA, Stern E. Transit time, trailing time, and cerebral blood flow during brain activation: measurement using multislice, pulsed spin-labeling perfusion imaging. Magn Reson Med. 2000; 44:680–685. [PubMed: 11064401]

26. Buxton RB, Frank LR, Wong EC, Siewert B, Warach S, Edelman RR. A general kinetic model for quantitative perfusion imaging with arterial spin labeling. Magn Reson Med. 1998; 40:383–396. [PubMed: 9727941]

27. Alsop DC, Detre JA. Reduced transit-time sensitivity in noninvasive magnetic resonance imaging of human cerebral blood flow. J Cereb Blood Flow Metab. 1996; 16:1236–1249. [PubMed: 8898697]

28. Hendrikse J, Lu H, van der Grond J, Van Zijl PC, Golay X. Measurements of cerebral perfusion and arterial hemodynamics during visual stimulation using TURBO-TILT. Magn Reson Med. 2003; 50:429–433. [PubMed: 12876722]

29. Bangash MF, Xie A, Skatrud JB, Reichmuth KJ, Barczi SR, Morgan BJ. Cerebrovascular response to arousal from NREM and REM sleep. Sleep. 2008; 31:321–327. [PubMed: 18363307]

30. Lu H, Clingman C, Golay X, van Zijl PC. Determining the longitudinal relaxation time (T1) of blood at 3.0 Tesla. Magn Reson Med. 2004; 52:679–682. [PubMed: 15334591]

31. An H, Lin W, Celik A, Lee YZ. Quantitative measurements of cerebral metabolic rate of oxygen utilization using MRI: a volunteer study. NMR Biomed. 2001; 14:441–447. [PubMed: 11746936]

32. Spilt A, Box FM, van der Geest RJ, Reiber JH, Kunz P, Kamper AM, Blauw GJ, van Buchem MA. Reproducibility of total cerebral blood flow measurements using phase contrast magnetic resonance imaging. J Magn Reson Imaging. 2002; 16:1–5. [PubMed: 12112496]

33. Moore, KL.; Dalley, AF. Clinically Oriented Anatomy. Lippincott Williams & Wilkins; 1999.

34. Wright GA, Hu BS, Macovski A. Estimating oxygen saturation of blood in vivo with MR imaging at 1.5 T. J Magn Reson Imaging. 1991; 1:275–283. [PubMed: 1802140]

35. Oja JM, Gillen JS, Kauppinen RA, Kraut M, van Zijl PC. Determination of oxygen extraction ratios by magnetic resonance imaging. J Cereb Blood Flow Metab. 1999; 19:1289–1295. [PubMed: 10598932]

36. Golay X, Silvennoinen MJ, Zhou J, Clingman CS, Kauppinen RA, Pekar JJ, van Zijl PC. Measurement of tissue oxygen extraction ratios from venous blood T(2): increased precision and validation of principle. Magn Reson Med. 2001; 46:282–291. [PubMed: 11477631]

37. Haacke EM, Lai S, Reichenbach JR, Kuppusamy K, Hoogenraad FG, Takeichi H, Lin W. In vivo measurement of blood oxygen saturation using magnetic resonance imaging: a direct validation of the blood oxygen level dependent concept in functional brain imaging. Human Brain Mapping. 1997; 5:341–346. [PubMed: 20408238]

38. Fernandez-Seara MA, Techawiboonwong A, Detre JA, Wehrli FW. MR susceptometry for measuring global brain oxygen extraction. Magn Reson Med. 2006; 55:967–973. [PubMed: 16598726]

39. Yablonskiy DA, Haacke EM. Theory of NMR signal behavior in magnetically inhomogeneous tissues: the static dephasing regime. Magn Reson Med. 1994; 32:749–763. [PubMed: 7869897]

40. An H, Lin W. Impact of intravascular signal on quantitative measures of cerebral oxygen extraction and blood volume under normo- and hypercapnic conditions using an asymmetric spin echo approach. Magn Reson Med. 2003; 50:708–716. [PubMed: 14523956]

41. He X, Yablonskiy DA. Quantitative BOLD: mapping of human cerebral deoxygenated blood volume and oxygen extraction fraction: default state. Magn Reson Med. 2007; 57:115–126. [PubMed: 17191227]

42. He X, Zhu M, Yablonskiy DA. Validation of oxygen extraction fraction measurement by qBOLD technique. Magn Reson Med. 2008; 60:882–888. [PubMed: 18816808]

43. Stefanovic B, Pike GB. Human whole-blood relaxometry at 1.5 T: Assessment of diffusion and exchange models. Magn Reson Med. 2004; 52:716–723. [PubMed: 15389952]

44. Silvennoinen MJ, Clingman CS, Golay X, Kauppinen RA, van Zijl PC. Comparison of the dependence of blood R2 and R2* on oxygen saturation at 1.5 and 4.7 Tesla. Magn Reson Med. 2003; 49:47–60. [PubMed: 12509819]

45. Chanarin, I.; Brozovic, M.; Tidmarsh, E.; Waters, D. Blood and its Disease. New York: Churchill Livingstone; 1984.

46. Powers WJ, Grubb RL Jr, Darriet D, Raichle ME. Cerebral blood flow and cerebral metabolic rate of oxygen requirements for cerebral function and viability in humans. J Cereb Blood Flow Metab. 1985; 5:600–608. [PubMed: 3877067]

47. Fox PT, Raichle ME, Mintun MA, Dence C. Nonoxidative glucose consumption during focal physiologic neural activity. Science. 1988; 241:462–464. [PubMed: 3260686]

48. Perlmutter JS, Powers WJ, Herscovitch P, Fox PT, Raichle ME. Regional asymmetries of cerebral blood flow, blood volume, and oxygen utilization and extraction in normal subjects. J Cereb Blood Flow Metab. 1987; 7:64–67. [PubMed: 3492507]

49. Ishii K, Sasaki M, Kitagaki H, Sakamoto S, Yamaji S, Maeda K. Regional difference in cerebral blood flow and oxidative metabolism in human cortex. J Nucl Med. 1996; 37:1086–1088. [PubMed: 8965174]

50. Hattori N, Bergsneider M, Wu HM, Glenn TC, Vespa PM, Hovda DA, Phelps ME, Huang SC. Accuracy of a method using short inhalation of (15)O-O(2) for measuring cerebral oxygen extraction fraction with PET in healthy humans. J Nucl Med. 2004; 45:765–770. [PubMed: 15136624]

51. Ito H, Kanno I, Fukuda H. Human cerebral circulation: positron emission tomography studies. Ann Nucl Med. 2005; 19:65–74. [PubMed: 15909484]

52. Coles JP, Fryer TD, Bradley PG, Nortje J, Smielewski P, Rice K, Clark JC, Pickard JD, Menon DK. Intersubject variability and reproducibility of 15O PET studies. J Cereb Blood Flow Metab. 2006; 26:48–57. [PubMed: 15988475]

53. Ibaraki M, Miura S, Shimosegawa E, Sugawara S, Mizuta T, Ishikawa A, Amano M. Quantification of cerebral blood flow and oxygen metabolism with 3-dimensional PET and 15O: validation by comparison with 2-dimensional PET. J Nucl Med. 2008; 49:50–59. [PubMed: 18077532]

54. Hayashi T, Suzuki A, Hatazawa J, Hadeishi H, Shirane R, Tominaga T, Yasui N. Postoperative changes of cerebral circulation and metabolism in the acute stage of low-grade aneurysmal subarachnoid hemorrhage. Neurol Res. 2008; 30:678–683. [PubMed: 18631432]

Appendix: Effect of Hct variations on CMRO2 estimation

Numerical simulations were performed to assess the effect of Hct variations on the estimated $CMRO_2$ values. In the estimation of $CMRO_2$ in Eq. 1, the value of Hct is needed for the determination of two parameters. First, C_a is linearly dependent on Hct, as more hemoglobin means a greater oxygen-carrying capacity of the blood (the amount of oxygen dissolved in the blood is negligible). Second, the calibration plot to convert blood T_2 into Y_v is affected by Hct. That is, the blood T2 is dependent on both Y_v and Hct. Such a dependence has been established previously for 1.5T (34,43) and 4.7T (44), and more recently for 3T (24). Typical Hct values for normal subjects are within the range of 0.38 to 0.50 (45). In the present study, we did not perform blood sampling to measure Hct on a subject-by-subject basis. Instead, the Hct was assumed to be 0.44 for all subjects. Therefore, it is important to estimate the error in $CMRO_2$ when the true Hct is different from the assumed value.

The simulations start with a set of assumptions on true parameter values: Y_a=100%, Y_v=61.5%, CBF=48.3ml/100g/min, oxygen-carrying capacity of 1 gram of hemoglobin=55.6 μmol of oxygen. Hct varies from 0.38 to 0.50 at an interval of 0.01. For each Hct value, the true $CMRO_2$ was calculated using Eq. 1. The venous blood T2 was also calculated using the Hct-specific coefficients established by Zhao et al. (24). These simulated data were then processed using our standard data processing strategies, in which Hct was always assumed to be 0.44. The estimated Y_a-Y_v, C_a, and $CMRO_2$ was computed and compared to the true values. Fig. 6 plots the bias caused by the incorrect assumption of Hct value. It can be seen that the terms Y_a-Y_v and C_a are biased in the opposite directions and their effects on $CMRO_2$ were partly cancelled out. As a result, the bias in $CMRO_2$ is mild.
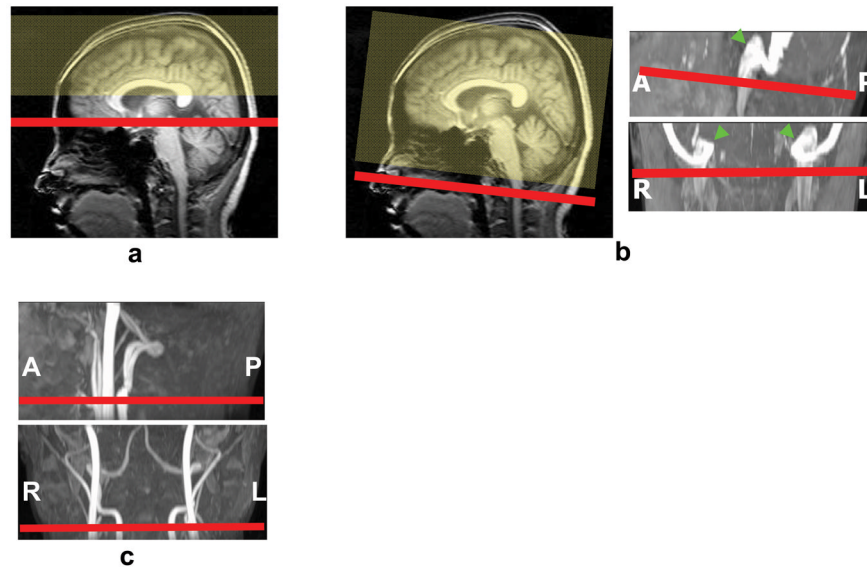
Fig. 1.
Slice positions for the scans in the CMRO$_2$ measurements. (a) Venous oxygenation in SS was estimated by imaging the SS in the occipital region (red) while tagging the venous blood upstream to that location (yellow). (b) The planning of the IJV scan was based on a mid-sagittal survey image and a venogram, and the imaging slice was positioned immediately below the jugular bulb (arrows). (c) Phase-contrast MRI was planned on an angiogram and the slice orientation was perpendicular to internal carotid and vertebral arteries.
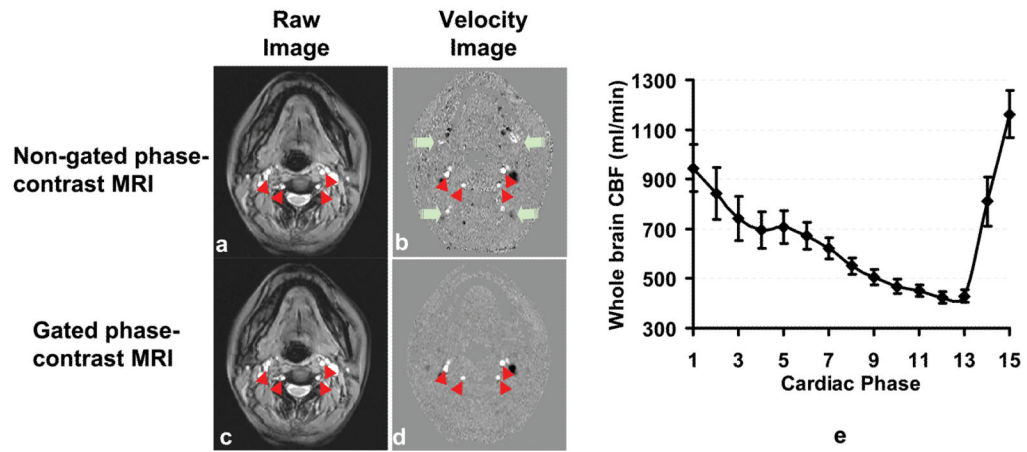
Fig. 2.
Comparison of gated and non-gated phased-contrast MRI. The raw images (a and c) of these two sequences are similar. However, the velocity map (b) of the non-gated scan shows some ghosting artifacts (green arrows) along the phase-encoding direction (anterior-posterior), due to flow pulsation in large vessels. Red arrowheads indicate the internal carotid and vertebral arteries. (e) Whole brain CBF (summation of internal carotid and vertebral arteries) at different cardiac phases during a heart beat (n=5). The averaged value of all the cardiac phases is comparable the non-gated value (p=0.53). The R-R interval was evenly divided into 15 phases. Error bars indicate the standard errors of mean.
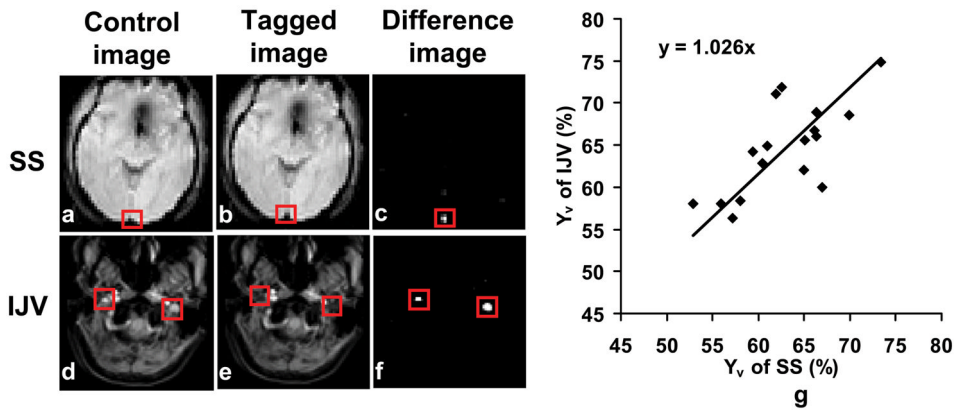
Fig. 3.
Results of TRUST MRI at SS and IJV. The control and tagged images appear similar, while the different images show clear delineation of the tagged vessels. The red boxes illustrate the manually drawn ROI for quantitative analysis. (g) Correlation between estimated venous oxygenation in SS and in IJV (n=17). A significant correlation (cc=0.71, p=0.0015) was found between them. The line is the fitting of the data to y=ax.
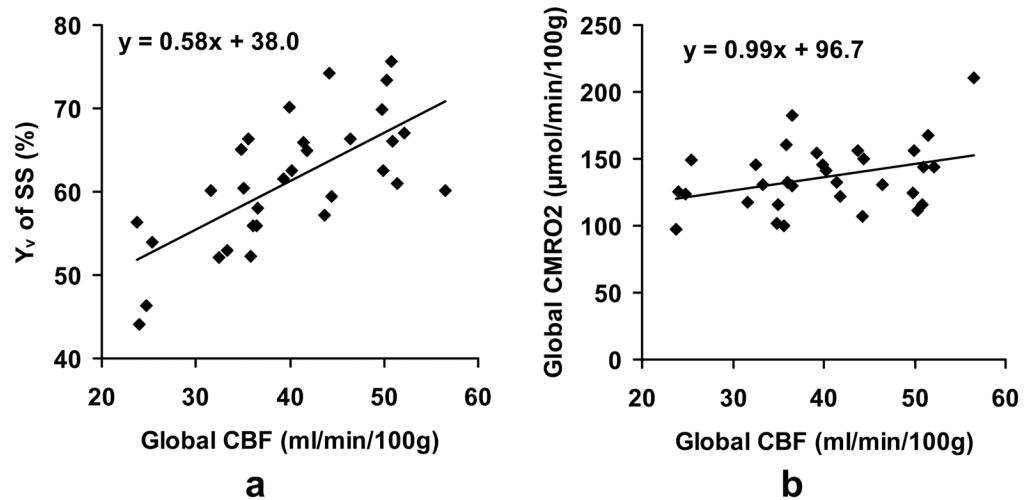
Fig. 4.
Correlation between different physiologic parameters across subjects. (a) Scatter plot between global CBF and venous oxygenation (n=31, cc=0.65, p<0.0001). Each dot in the plot represents data from one subject. It can be seen that individual with higher blood flow tends to have higher venous oxygenation, which corresponds to lower oxygen extraction fraction. The line indicates the linear fitting of the data. (b) Scatter plot between global CBF and CMRO2. A weak correlation (cc=0.41, p=0.0222) is observed.
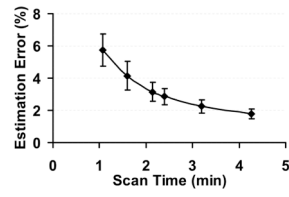
Fig. 5.
TRUST MRI measurement accuracy as a function of scan duration. The measurement accuracy is quantified by the estimation error from the goodness-of-fit analysis.
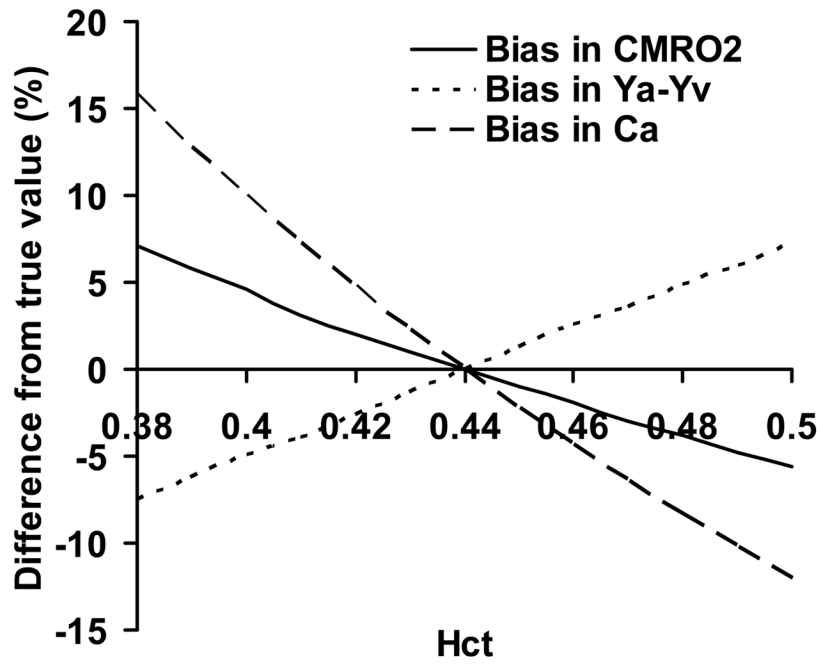
Fig. 6.
Simulation results of the effect of Hct. Variations in Hct cause biases in the estimated Y_a-Y_v and C_a. These two effects are opposite in directions. Thus, the bias in the estimated $CMRO_2$ is smaller in amplitude. All values are shown in relative changes, i.e. (estimated value-true value)/true value $\times$ 100%.

Table 1

Summary of results for $CMRO_2$ measurement (mean±SD, n=17).

$CMRO_2$ using Y_v in SS (μmol/min/100g)	$CMRO_2$ using Y_v in IJV (μmol/min/100g)	Global CBF (ml/min/100g)	Intracranial Volume (ml)
132.1±20.0	127.6±20.9	43.3±7.1	1608.1±175.3

Table 2

A review of literature $CMRO_2$ values in normal subjects.

Study	$CMRO_2$ value[*] (μmol/min/100g)	Subject age (years)	Number of subjects
Mintun et al. 1984 (7)	131 (95–201)	23–40	5
Powers et al. 1985 (46)	130 (63–219)	18–84	24
Fox et al. 1988 (47)	150	19–26	5
Perlmutter et al. 1987 (48)	118 (109–134)	20–84	32
Ishii et al. (49)	157 (143–184)[Δ]	42–73	15
Hattori et al. 2004 (50)	127 (105–171)	21–46	16
Ito et al. 2005 (51)	139	n/a	70
Coles et al. 2006 (52)	125	18–60	10
Ibaraki et al. 2008 (53)	147 (114–181))[Δ]	21–24	8
Hayashi et al. 2008 (54)	147	40–69	16

[*] - values in the parenthesis are ranges across subjects/brain regions.

[Δ] - gray matter values.